ELSEVIER

Contents lists available at ScienceDirect

# Scripta Materialia

journal homepage: www.journals.elsevier.com/scripta-materialia





# The effects of ultrasonic vibration on Portevin–Le Chatelier (PLC) effect and stress-strain behavior in aluminum alloy 2024

Jiarui Kang\*, Xun Liu\*, Tianzhao Wang

Welding Engineering, Department of Material Science and Engineering, The Ohio State University, 1248 Arthur E Adams Dr, Columbus, OH 43221, USA

#### ARTICLE INFO

Keywords: Aluminum alloy Portevin-Le Chatelier effect Digital image correlation Ultrasonic softening Dynamic strain aging

#### ABSTRACT

The effect of ultrasonic vibration on the stress-strain behavior and the Portevin–Le Chatelier (PLC) effect in aluminum alloy 2024 O temper and T4 were investigated based on ultrasonically assisted micro-tensile tests. Flow stress in both heat treatments was found to be decreasing when ultrasonic vibration is applied. A higher percentage of stress reduction and the residual softening effect was observed in O temper. High-speed digital image correlation reveals the enhanced PLC bands in both heat treatments. While no PLC band was observed in T4 originally, clear PLC bands appear with applied ultrasound. Spatio-temporal analysis revealed that in both O temper and T4 conditions, the critical strain of the PLC effect decreases under ultrasonic vibration. In addition, a higher strain rate magnitude was observed in conditions with ultrasonic vibration.

Ultrasonic vibration has been applied to improve various metal forming and welding processes [1], such as ultrasonically assisted (UA) wire drawing [2], extrusion [3], incremental sheet forming [4], and friction stir welding [5]. The ultrasonic softening effect, i.e., the reduction of material flow stress during plastic deformation, has been reported consistently. This softening effect is generally explained by the enhanced dislocation motion and annihilation and therefore reduced dislocation density under oscillating stress [6,7].

While the stress-strain behavior of metal under the effect of ultrasonic vibration has been studied extensively, few open works discuss the ultrasonic influence on the deformation where the collective movement of dislocations plays an important role. One such example is the Portevin-Le Chatelier (PLC) effect [8], where intermittent and self-organized dislocation activity is revealed by acoustic emission measurements [9,10]. The PLC effect is manifested in serrations in the stress-strain curve and localized deformation bands [11-13]. The mechanism of the PLC effect is generally ascribed to dynamic strain aging [14-18]. When mobile dislocations are arrested at obstacles, such as forest dislocation, grain boundaries, and precipitates, during the waiting time for thermally activated dislocation motion, the solute atoms diffuse towards the dislocations and cause additional pinning. The pining and the subsequent abrupt break-away of dislocations macroscopically manifest as the PLC band. In the pioneering work by Brynk and Kurzydlowski [19], the change of PLC band morphology was observed with the application of ultrasonic vibration in the frequency of 2.5 and 5 MHz. However, the phenomenon was only observed below a stress level of 160 MPa, potentially because of the limited ultrasonic power in their study.

In this study, with the aid of digital image correlation (DIC), the plastic behavior of aluminum alloy 2024 in both T4 and O temper was studied systematically by micro-tensile testing with power ultrasound. Ultrasonically induced PLC effect in aluminum alloy 2024 T4 is reported for the first time. The gauge length of miniature dog bone specimens was designed as 1.6 mm, more than one order of magnitude smaller than that of a 20 kHz ultrasonic wavelength in aluminum. This ensures that vibration amplitude along the sample gauge is relatively uniform and therefore does not introduce stress/strain concentration spots.

Commercially available aluminum alloy AA2024 was used in this research, with copper and magnesium being the main alloying elements. Micro-tensile tests were performed on two heat treatments of AA2024, i. e., annealed O temper and T4. T4 state is primarily strengthened by Guinier-Preston (GP) zones and is obtained by solution heat treatment, water quench, and subsequently natural aging at room temperature for 5 days, following AMS standard 2772G [20]. Miniature specimens were placed in grips with mating geometry for tensile test. One of the grips is connected to a high-resolution linear motor and the other is mounted to a 20 kHz piezoceramic ultrasonic transducer powered by a Dukane IQ AIM power source with a maximum power output of 3.6 kW. The vibration amplitude at the tip of the UA grip is measured using a Polytec laser doppler vibrometer. The variation of ultrasonic amplitude with

E-mail addresses: kang.1057@osu.edu (J. Kang), liu.7054@osu.edu (X. Liu).

<sup>\*</sup> Corresponding authors.

power percentage is given in Table 1.

Micron-scale speckle pattern was prepared on the sample surface for DIC analysis. Additional details on the micro-tensile testing are given in Refs. [21,22]. The tensile strain rate is 0.06/s. A control program is developed using LabView and Arduino to initiate ultrasonic vibration at a certain tensile strain and hold for 2 seconds during the tests with UA. For each heat treatment condition, three levels of vibration amplitude were tested. Five samples were tested in each condition. Virtual extensometers in DIC were used to measure the engineering strain along the sample gauge.

Fig. 1 (a) and (b) show the stress-strain curves for AA2024 O temper and T4 under different conditions. AA2024 in these two heat treatments behave very differently. O temper (black line in Fig. 1 a) yields at 63.1 MPa, which is significantly lower than that of T4 (black line in Fig. 1 b), at 222.3 MPa. AA2024 O also hardens at a lower rate and reaches an ultimate tensile strength (UTS) of 169.1 MPa. In contrast, AA2024 T4 shows a UTS of 380.0 MPa and exhibits smaller elongation. This is attributed to the difference in the microstructure. Mainly GP zones form during room temperature aging in T4, which provides moderate strengthening. In contrast, in the annealed O temper condition, solute atoms precipitate out and form equilibrium phases Al<sub>2</sub>Cu and Al<sub>2</sub>CuMg. During annealing, the size and spacing L of secondary phases increase while the density decreases. This reduces the Orowan strengthening effect  $\tau_{Orowan} = 0.84Gb/L$ , where G and b are the shear modulus and Burgers vector magnitude, respectively.

The UA responses of these two materials are also considerably different. For T4, there is no noticeable change in the hardening behavior with UA. After a transient decrease in stress, the stress-strain curves with UA follow the same trend as the one with no UA. When UA stops, the stress under all three UA amplitudes jumps back to the same level as the one without UA. In contrast, O temper behaves differently both during and after UA stops. There is a notable decrease in the hardening rate in 25% and 30% UA compared to 20% UA. In addition, residual softening is observed in O temper, i.e., flow stress stays at a lower level after UA is off. The level of residual softening is also found to increase with ultrasonic amplitude.

The relationship between stress reduction and vibration amplitude for AA2024 O temper and T4 is further evaluated. The flow stress with UA is calculated as the mean value of the oscillation range  $\sigma_{UA} = (\sigma_{UA}^{max} +$  $\sigma_{UA}^{min})/2$ . Relative reductions are calculated as  $(\sigma_{No~UA}-\sigma_{UA})/\sigma_{No~UA}$  at 8% engineering strain for both material states and are shown in Fig. 1 (c). For both O temper and T4, the relative stress reductions increase with ultrasonic vibration amplitude. O temper shows significant stress reduction, increasing from 32.4% at 4.1 µm amplitude to 55.3% at 6.3 μm amplitude. In contrast, T4 shows a considerably lower level of relative stress reduction. At 6.3 µm amplitude, the relative reduction in stress of T4 is 17.5%, around one-third of that in O temper. The change in stress-strain behavior under UA is also evaluated from an energy perspective. The stress-strain curves with UA were fitted using the smoothing spline fit in MATLAB to reflect the mean value of the oscillation in stress. The fitted curves for O temper and T4 are shown in Fig. 1 (d) and (e), respectively, which are then compared to the ones obtained with no UA. The differences in the areas under the curves give the change in strain energy density as a result of UA and are compared against the energy density of acoustic wave, which can be expressed as  $\xi_{UA} = 4\pi^2 f^2 A^2 \rho$  and varies proportionally with the square of vibration amplitude, where f and A are ultrasonic frequency and amplitude, and  $\rho$ is the density of media. As shown in Fig. 1 (f), the reductions in strain energy density for both heat treatment conditions increase with the square of amplitude in a linear way. The trend lines for O temper and T4

 Table 1

 Variation of ultrasonic amplitude with power input.

Power source energy input (%)	20	25	30
Vibration amplitude (μm)	4.1	5.2	6.3

are comparable in slope, which indicates the increment of softening is determined by the acoustic energy input. However, the intercept of the O temper curve is considerably higher than that of T4. This is attributed to the difference in microstructure and how it influences the interaction between ultrasonic vibration and dislocations.

DIC analysis shows clear PLC band formation and propagation during the tensile test of AA2024 O temper, as shown in Fig. 2 (a). The band angle to tensile direction is measured as  $56\text{-}60^\circ$ . To better visualize the UA effect on PLC, spatial-temporal analysis was performed, where the line profile of strain rate magnitude is extracted and plotted against position along the sample gauge section and engineering strain.

Fig. 2 (b-e) compares the spatial-temporal contour plots for AA2024 O temper samples tested at different UA amplitudes. Y axis denotes the position along the gauge section in the reference image which is taken prior to testing. X axis is the engineering strain. Accordingly, the plot shows the evolution and movement of localized deformation regions along the specimen gauge as strain increases. Fig. 2 (b) shows the strain rate contour without UA. PLC bands are visible starting from around 6.0% engineering strain. The propagation is unidirectional and continuous, from the UA grip side towards the moving grip side, except for the one close to necking. The strain rate contours with different ultrasonic amplitudes are shown in Fig. 2 (c-e), with the strain values where UA was switched on and off marked in white dashed lines. It is worth noting that the critical strain where the PLC effect initiates has decreased considerably to around 4.1%, 4.2%, and 4.0% with 20%, 25%, and 30% ultrasonic power, respectively.

Fig. 3 (a) and (b) show the strain rate contour maps for AA2024 T4 at 8.5% strain with no UA and 30% UA, respectively. While no PLC band is observed without UA, clear PLC bands appear with the UA application. This can be better visualized in the contour plots shown in Fig. 3 (c-f).

As shown in Fig. 3 (c), there is no visible PLC band present throughout the entire test. This is well documented for the T4 state and attributed to the formation of GP zones during natural aging [23]. Normally, the alloying elements diffuse towards dislocations that are temporarily arrested at forest dislocations and form an atmosphere that further pin dislocations [24]. With the presence of GP zones, vacancies and alloying elements can be trapped by the strain field around GP zones, which slows down solute atoms diffusion considerably [25]. Therefore, fewer solute atoms can pin dislocations, and the PLC effect only occurs when sufficient vacancies are generated with a large amount of plastic strain [26]. As a result, the critical strain to induce PLC increases as room temperature aging time prolongs [23]. In a fully room temperature aged T4 state, no PLC effect is observed. This suggests that the critical strain of PLC exceeds the strain of necking. However, with the presence of ultrasonic vibration, clear PLC band formation and propagation along the sample gauge are observed in Fig. 3 (d-f). This suggests that ultrasonic vibration influences the interaction between dislocation and obstacles during the deformation. With the increase in strain, discontinuous and subsequently continuous banding is observed. The critical strains were found to be 7.1%, 6.9%, and 5.3% under 20%, 25%, and 30% UA, decreasing monotonically with UA amplitude. It should also be noted that after UA is switched off, the propagation of the PLC band continues, which indicates irreversible microstructural change induced by UA. In addition, it is worth noting that the effect of UA on PLC is consistent throughout the entire testing regardless of stress level. This is attributed to the sufficiently high ultrasonic power in this study. As a comparison, the effect of UA on PLC morphology was only observed below 160 MPa in the work of Brynk and Kurzydlowski [19].

In testing conditions where PLC bands are visible, the traveling velocity of the PLC band, illustrated by the slope in the spatio-temporal plots, decreases with increasing strain. This matches with the experimental observations of McCormick et al. [27], and Ranc and Wagner [28]. The decrease in band velocity can be attributed to the increase of dislocation density as deformation proceeds and materials being strain hardened. Therefore, mobile dislocations are more likely to be arrested by sessile dislocation and other obstacles. The waiting time that

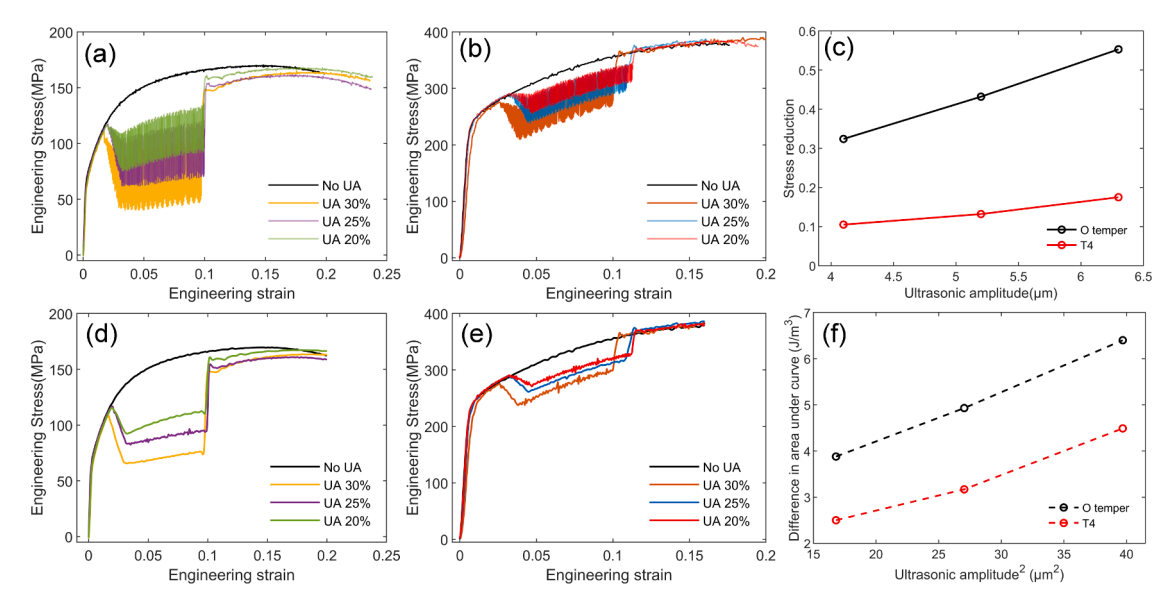


Fig. 1. Stress-strain curves for AA2024 (a) O temper and (b) T4, (c) variation of relative stress reduction with ultrasonic amplitude, (d) and (e) smoothing spline fit of (a) and (b), (f) variation of the difference in the area under stress-strain curve against the square of vibration amplitude.

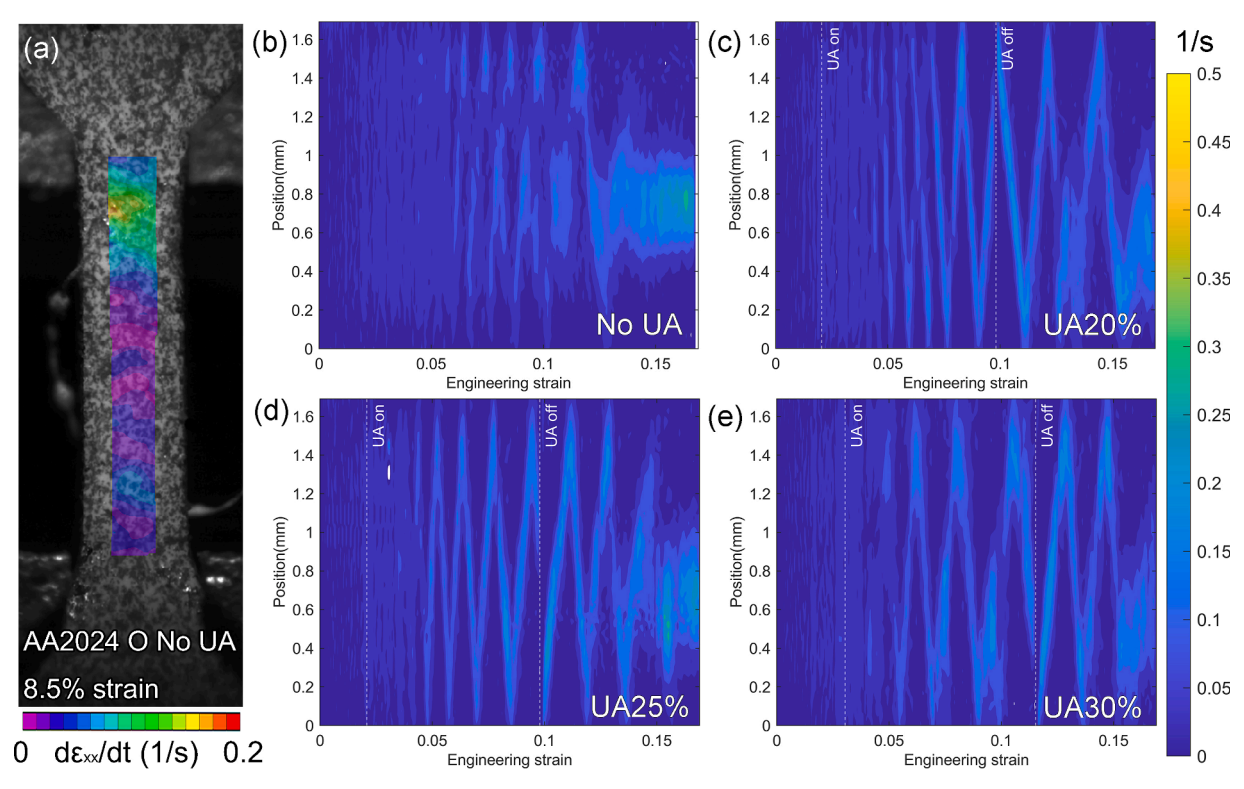


Fig. 2. DIC results of AA2024 O temper (a) strain rate map at 8.5% strain, (b-e) spatial-temporal contour plots of strain rate under different conditions.

dislocations spend at obstacles increases according to  $t=b\rho_m/\dot{\epsilon}\sqrt{\rho_f}$ , where  $\dot{\epsilon}$  is plastic strain rate,  $\rho_m$  and  $\rho_f$  are the densities of mobile and forest dislocation, respectively [29,13].

In both AA2024 O and T4 states, higher strain rate magnitude in the PLC bands is observed with UA from the spatial-temporal contour plots. The maximum value of strain rates along the gauge section at different strains are extracted and compared quantitatively. The results are shown in Fig. 4 (a) and (b) for O temper and T4, respectively, with the regions of UA zoomed in. In both material states, the maximum strain rate values are higher with UA. This effect is more significant in the T4 condition since in the no UA condition deformation is uniform, and no PLC band is

visible.

It is noticeable that in both heat treatments, PLC bands disappear briefly when UA is off, as shown in Figs. 2 and 3. Correspondingly, an instantaneous decrease in maximum strain rate can be noticed in Fig. 4. This is attributed to the sudden increase in material flow stress when UA is stopped, as shown in the stress-strain curves in Fig. 1. As a result, momentarily higher resistance is imposed on the tensile crosshead, which results in a decrease in strain rate. Subsequently, the strain rate on the sample increases back to the originally imposed value. During this time, the stress is observed to overshoot and then decrease to the new quasi-static state. This transient change in stress confirms the

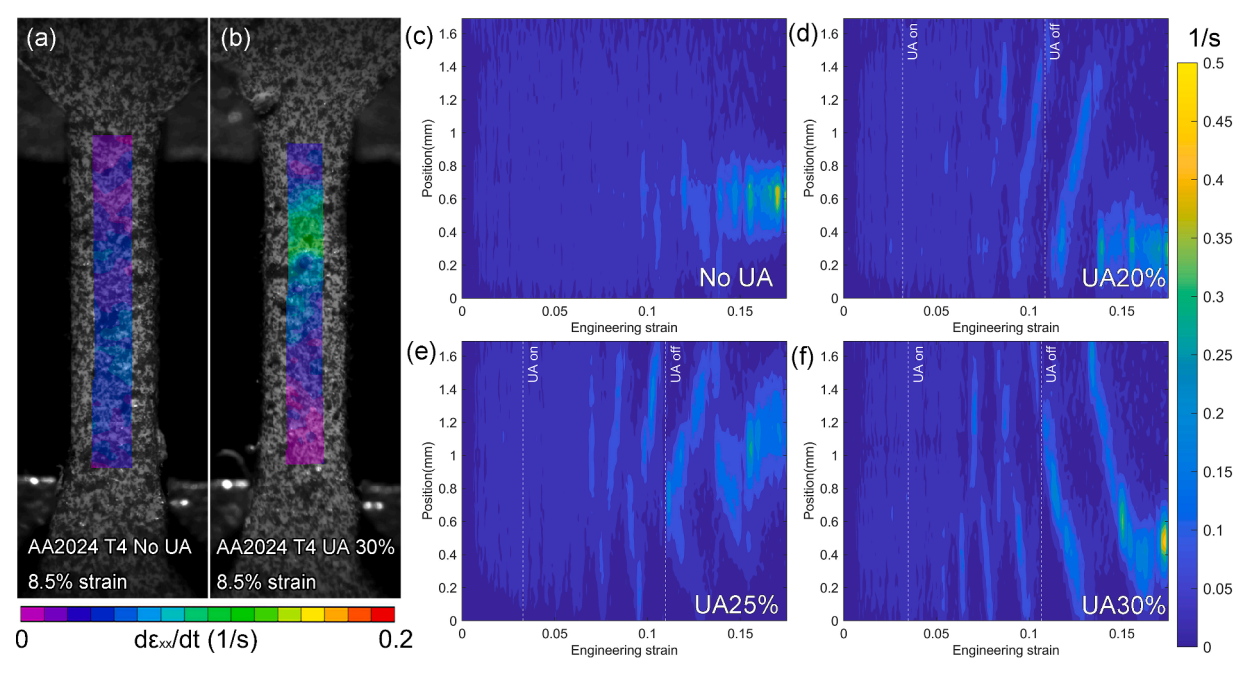


Fig. 3. DIC strain rate map at 8.5% strain of AA2024 T4 with (a) no UA and (b) UA, (c-f) spatial-temporal contour plots of strain rate under different conditions.

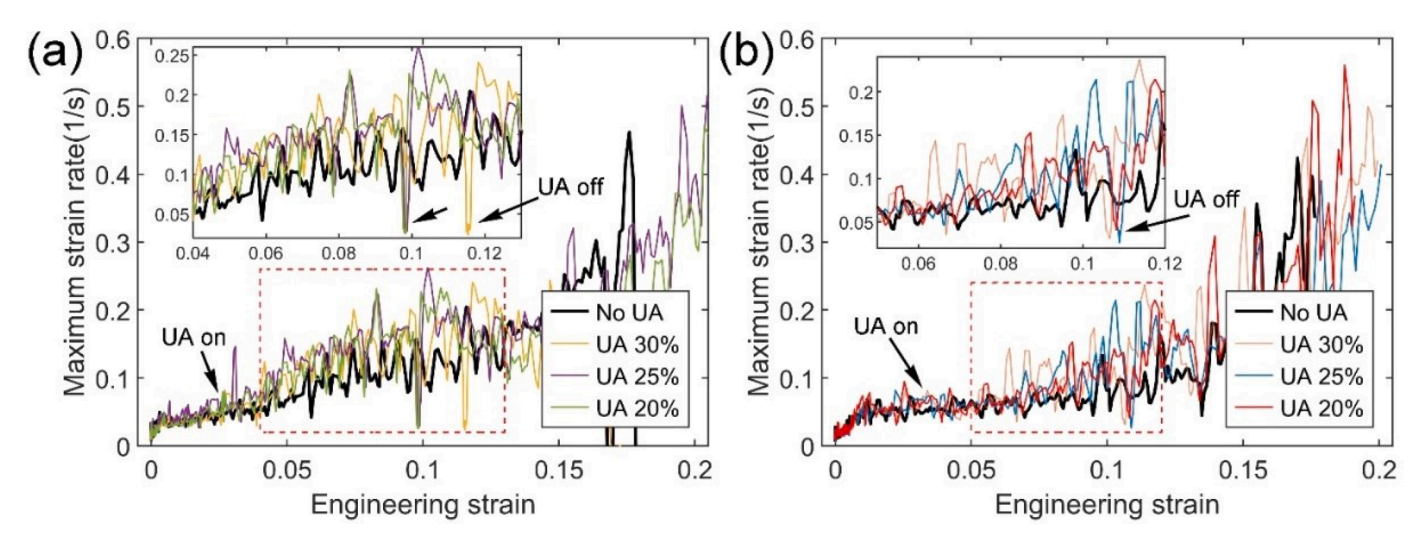


Fig. 4. Maximum strain rate along gauge section in AA2024 (a) O temper and (b) T4 under different conditions.

mechanism of dynamic strain aging [30–32], which predicts lower solute concentration at arrested dislocations at a higher strain rate. The change in solute concentration cannot happen instantly and therefore gives rise to the time-dependent behavior of flow stress.

The enhanced PLC effect under applied ultrasonic vibration can be attributed to the facilitated dislocation motion under oscillatory stress. Acoustic emission measurements of the PLC effect revealed that the macroscopic plastic instability is caused by the clustering of acoustic events, i.e., the synchronization of dislocation avalanches [33–35]. While discrete avalanches of dislocations also occur in smooth flow before critical strain [33], it does not lead to a macroscopic drop in stress because of the low and heterogeneous stress state in the early stage of deformation. The dislocation avalanche generated in local stress concentration is not likely to trigger other nearby avalanche events. With the application of ultrasonic vibration, the mobility of dislocation is enhanced [6,7], which helps to homogenize the stress state in the material by promoting the motion of uncorrelated dislocations. As a result, a more uniformed material state is reached earlier, and a local avalanche

would trigger the synchronization of dislocation avalanches that leads to the observed macroscopic plastic instability.

It is worth noting that while the concentration of solute atoms decreases as equilibrium precipitates, Al<sub>2</sub>Cu and Al<sub>2</sub>CuMg, form in the anneal O temper state, these precipitates are large and incoherent to the matrix and therefore do not bind to vacancies as effectively as GP zones. As a result, remaining solute atoms and vacancies can still diffuse fast towards dislocations and cause the PLC effect [24].

In summary, the plastic behaviors of AA2024 O temper and T4 under ultrasonic vibration were studied in micro-tensile testing with the application of power ultrasound. The reduction in flow stress was observed in both heat treatments and the change in strain energy density varies linearly with ultrasonic energy density. With the aid of DIC, the enhancement of the PLC effect by ultrasonic vibration was observed for the first time. In both heat treatments, UA lowers the PLC critical strain and increases the maximum strain rate along the specimen gauge section. Specifically in AA2024 T4, while no PLC effect can be observed originally, clear PLC bands appear under UA and continue to propagate

even after ultrasonic vibration is switched off, indicating permanent microstructural change induced by UA, which will be investigated by TEM in future work.

#### **Declaration of Competing Interest**

The authors declare that they have no known competing financial interests or personal relationships that could have appeared to influence the work reported in this paper.

## Acknowledgment

This work was supported by National Science Foundation CMMI AM program [grant number: 2019238].

### Supplementary materials

Supplementary material associated with this article can be found, in the online version, at doi:10.1016/j.scriptamat.2022.115121.

#### References

- K.F. Graff, Ultrasonic Metal Forming: Materials, in: J.A. Gallego-Juárez, K.F. Graff (Eds.), Power Ultrasonics, Woodhead Publishing, Oxford, 2015, pp. 337–376.
- [2] K. Siegert, J. Ulmer, Superimposing ultrasonic waves on the dies in tube and wire drawing, J. Eng. Mater. Technol. Trans. ASME 123 (2001) 517–523.
- [3] C. Bunget, G. Ngaile, Influence of ultrasonic vibration on micro-extrusion, Ultrasonics 51 (2011) 606–616.
- [4] R. Cheng, N. Wiley, M. Short, X. Liu, A. Taub, Applying ultrasonic vibration during single-point and two-point incremental sheet forming, Procedia Manuf. 34 (2019) 186–192.
- [5] K. Park, Development and analysis of ultrasonic assisted friction stir welding process, University of Michigan, 2009.
- [6] K.W. Siu, A.H.W. Ngan, I.P. Jones, New insight on acoustoplasticity ultrasonic irradiation enhances subgrain formation during deformation, Int. J. Plast. 27 (2011) 788–800.
- [7] R.K. Dutta, R.H. Petrov, R. Delhez, M.J.M. Hermans, I.M. Richardson, A.J. Böttger, The effect of tensile deformation by in situ ultrasonic treatment on the microstructure of low-carbon steel, Acta Mater. 61 (2013) 1592–1602.
- [8] A. Portevin, F.Le Chatelier, Sur un phénomène observé lors de l'essai de traction d'alliages en cours de transformation, C. R. Acad. Sci. Paris 176 (1923) 507–510.
- [9] M.A. Lebyodkin, N.P. Kobelev, Y. Bougherira, D. Entemeyer, C. Fressengeas, V. S. Gornakov, T.A. Lebedkina, I.V Shashkov, On the similarity of plastic flow processes during smooth and jerky flow: statistical analysis, Acta Mater. 60 (2012) 3729–3740
- [10] T.A. Lebedkina, Y. Bougherira, D. Entemeyer, M.A. Lebyodkin, I.V Shashkov, Crossover in the scale-free statistics of acoustic emission associated with the Portevin-Le Chatelier instability, Scr. Mater. 148 (2018) 47–50.
- [11] F. Chmelík, A. Ziegenbein, H. Neuhäuser, P. Lukáč, Investigating the Portevin-Le Châtelier effect by the acoustic emission and laser extensometry techniques, Mater. Sci. Eng. A 324 (2002) 200–207.

- [12] H. Ait-Amokhtar, P. Vacher, S. Boudrahem, Kinematics fields and spatial activity of Portevin–Le Chatelier bands using the digital image correlation method, Acta Mater 54 (2006) 4365–4371.
- [13] L.P. Kubin, Y. Estrin, Evolution of dislocation densities and the critical conditions for the Portevin-Le Châtelier effect, Acta Metall. Mater. 38 (1990) 697–708.
- [14] P. Penning, Mathematics of the portevin-le chatelier effect, Acta Metall. 20 (1972) 1169–1175.
- [15] P.G. McCormigk, A model for the Portevin-Le Chatelier effect in substitutional alloys, Acta Metall. 20 (1972) 351–354.
- [16] R.C. Picu, D. Zhang, Atomistic study of pipe diffusion in Al–Mg alloys, Acta Mater. 52 (2004) 161–171.
- [17] P. Hähner, On the physics of the Portevin-Le Châtelier effect part 2: from microscopic to macroscopic behaviour, Mater. Sci. Eng. A 207 (1996) 216–223.
- [18] Y. Estrin, L.P. Kubin, Collective dislocation behaviour in dilute alloys and the Portevin—Le Chatelier effect, J. Mech. Behav. Mater. 2 (1989) 255–292.
- [19] T. Brynk, K.J. Kurzydlowski, Coupling of ultrasounds with the Portevin–Le Chatelier serrations as observed in aluminium-magnesium alloy in mini-samples tensile tests, Scr. Mater. 174 (2020) 14–18.
- [20] AMS D Nonferrous Alloys. Committee, Heat Treatment of Aluminum Alloy Raw Materials, (2016).
- [21] J. Kang, X. Liu, M. Xu, Plastic deformation of pure copper in ultrasonic assisted micro-tensile test, Mater. Sci. Eng. A 785 (2020), 139364.
- [22] J. Kang, X. Liu, S.R. Niezgoda, Crystal plasticity modeling of ultrasonic softening effect considering anisotropy in the softening of slip systems, Int. J. Plast. 156 (2022), 103343.
- [23] H. Jiang, Q. Zhang, X. Wu, J. Fan, Spatiotemporal aspects of the Portevin-Le Chatelier effect in annealed and solution-treated aluminum alloys, Scr. Mater. 54 (2006) 2041–2045.
- [24] E. Pink, The effect of precipitates on characteristics of serrated flow in AlZn5Mg1, Acta Metall. 37 (1989) 1773–1781.
- [25] J. Chen, L. Zhen, L. Fan, S. Yang, S. Dai, W. Shao, Portevin-Le Chatelier effect in Al-Zn-Mg-Cu-Zr aluminum alloy, Trans. Nonferrous Met. Soc. China 19 (2009) 1071–1075.
- [26] D. Thevenet, M. Milha-Touati, A. Zeghloul, The effect of precipitation on the Portevin-Le Chatelier effect in an Al-Zn-Mg-Cu alloy, Mater. Sci. Eng. A 266 (1999) 175–182
- [27] P.G. McCormick, S. Venkadesan, C.P. Ling, Propagative instabilities: an experimental view, Scr. Metall. Mater. 29 (1993) 1159–1164.
- [28] N. Ranc, D. Wagner, Some aspects of Portevin-Le Chatelier plastic instabilities investigated by infrared pyrometry, Mater. Sci. Eng. A 394 (2005) 87–95.
- [29] Z. Jiang, Q. Zhang, H. Jiang, Z. Chen, X. Wu, Spatial characteristics of the Portevin-Le Chatelier deformation bands in Al-4at%Cu polycrystals, Mater. Sci. Eng. A. 403 (2005) 154-164
- [30] S.H.van den Brink, A.van den Beukel, P.G. McCormick, Strain rate sensitivity and the portevin-le chatelier effect in Au–Cu alloys, Phys. Status Solidi 30 (1975) 469–477.
- [31] P.G. McCormick, Y. Estrin, Transient flow behaviour associated with dynamic strain ageing, Scr. Metall. 23 (1989) 1231–1234.
- [32] P.G. McCormick, Theory of flow localisation due to dynamic strain ageing, Acta Metall. 36 (1988) 3061–3067.
- [33] N.P. Kobelev, M.A. Lebyodkin, T.A. Lebedkina, Role of self-organization of dislocations in the onset and kinetics of macroscopic plastic instability, Metall. Mater. Trans. A 48 (2017) 965–974.
- [34] Y. Bougherira, D. Entemeyer, C. Fressengeas, N.P. Kobelev, T.A. Lebedkina, M. A. Lebyodkin, The intermittency of plasticity in an Al3%Mg alloy, J. Phys. Conf. Ser. 240 (2010) 12009.
- [35] M.A. Lebyodkin, N.P. Kobelev, Y. Bougherira, D. Entemeyer, C. Fressengeas, T. A. Lebedkina, I.V Shashkov, On the similarity of plastic flow processes during smooth and jerky flow in dilute alloys, Acta Mater. 60 (2012) 844–850.